CHARACTERIZATION OF TURBULENT FLOW DOWNSTREAM OF A THREE-DIMENSIONAL AXISYMMETRIC BUMP

Ruolong Ma* and Roger L. Simpson
Department of Aerospace and Ocean Engineering
Virginia Polytechnic Institute and State University
Blacksburg, VA 24061, USA
simpson@aoe.vt.edu

ABSTRACT

The downstream wake development from a high momentum thickness Reynolds number ($Re_\theta \approx 7300$) boundary layer flow over an axisymmetric bump (with circular base) of height $H = 2\delta$ is experimentally studied using a four-sensor hot-wire probe. Three-component mean velocity, turbulence, velocity spectra, and two-point correlation measurements were made behind the bump within a distance from x/H =2.62 to 6.59 to fully document the turbulent flow structure and its streamwise evolution. Mean flow development, structure and decay of the turbulence, the contribution and distribution of low frequency turbulence fluctuations are presented.

INTRODUCTION

Although turbulent flow over hills has been studied over the last two decades, there is still a lack of detailed information and understanding of boundary layer flow over and downstream of three-dimensional bumps, especially for bumps over which complex vortical separations and reattachments occur on the lee side.

Flow over a three-dimensional surface-mounted geometry, which has recently been extensively studied both experimentally and computationally, concerns an axisymmetric bump (bump 3) with a circular base. The shape of the bump of height H is shown in figure 1 and the shape definition is given by Byun et al. (2004).

Willits and Boger (1999) first conducted an experimental and computational study for a turbulent boundary layer flow behind this bump shape, the boundary layer having a thickness, δ, or $0.5H$ at the bump center when the bump is absent. Measurements were made by using a five-hole probe and X-wire boundary layer probe at three streamwise locations, x/H=6.5, 11.5, and 16.5. However, the comparison of a RANS solution using a q-ω turbulence model for bump 3 showed poor agreement. The authors suggested more experimental measurements may be required to understand better the flow.

*Currently at: Center for Flow Physics and Control, Hessert Laboratory, University of Notre Dame, Notre Dame, IN 46556, USA, ruolong.ma.14@nd.edu

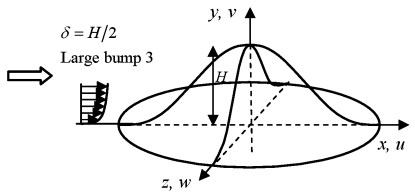

Figure 1. Shape of bump 3 (not to scale)

Simpson et al. (2001) and Byun et al. (2004) investigated the flow over the same bump through oil flow visualization, surface mean pressure, and downstream 3-velocity-component LDV measurements. The bump 3 was studied for two flow conditions, δ/H equals to 0.5 (large bump 3) and 1 (small bump 3 with a height of half of large bump 3). The oil flow visualization suggests that complex vortical separations occur over a large area on the lee side of large bump 3 and each bump has a different flow pattern. The downstream LDV measurements at a closer location for each bump (x/H =3.63 for large bump 3, x/H =3.26 for small bump 3) reveal that the separated flow merges into large streamwise mean vortices downstream for the large bump 3. Limited w spectra in low frequency range were also measured in the centerline and at the height of the mean vortex center for each bump and suggest that there are low frequency motion behind large bump 3.

Computational studies on the flow over large bump 3 include the LES computation by Patel et al. (2003) and RANS and LES work by Wang et al. (2004). Patel *et al.* explored the ability of a LES method to calculate this flow and found LES can reproduce qualitatively and in some case quantitatively the flow features. However, there is some difference in the downstream mean flow and stress data between the LDV and LES, also in the lee side where complex separation and reattachment occurs between LES and oil flow visualization. Wang et al. used RANS with five different anisotropy-resolving turbulence models. Although there are clearly subtle differences among the solutions, significant disagreement exists when they are compared with the LDV data. The calculated downstream wake flow is narrow with more intense turbulence and higher streamwise velocity deficit.

These experimental and computational studies all suggest that there are complicated structures and large scale organized unsteady motions in the separation region behind the bump. The lack of understanding and the inaccuracy of the turbulence models are the reasons that calculations fail to give satisfactory representation. It is thus necessary to investigate the detailed downstream development of the flow immediately behind the bump and the dynamic features including the large scale and organized shedding-like unsteadiness, and associated turbulence production, convection, and diffusion, etc. This information is critical for understanding the turbulence structure, improving the anisotropy-resolving turbulence models and LES calculations. The objectives of the current study are to provide information toward an improved understanding, and to provide an accurate and complete downstream flow picture for computation validation.

To achieve these objectives, extensive three-component hot-wire measurements of mean flow, velocity fluctuations, and spectra were made at different streamwise cross sections just behind the bump. Some two-point correlation measurements were also made to explore the turbulent structures. Spectral decomposition was used to separate the contributions from velocity fluctuations of different frequency ranges to examine the form and structure of turbulent flow. These measurements reveal in new detail the turbulent structure of the trailing vortices shed by each bump, the manner of their decay, turbulence kinetic energy level, the contribution of velocity fluctuations at different frequency range, as well as their distribution.

In this paper, only the measurement results of the large bump 3 are presented because of the space limit. Detailed presentation of the measurement results of all bumps will be given in future paper.

APPARATUS AND INSTRUMENTS

The bump height H is 78mm. The radius of the circular base of the bump is $2H$. The maximum slope of bump 3 is 37.7°.

The measurements were conducted in the AOE Department low speed boundary layer wind tunnel, which is shown in figure 2 and is described in detail by Devenport and Simpson (1990). The test section is a 6m long rectangular channel, which produces, for the no bump case, a flow of very nearly zero streamwise pressure gradient and thus an equilibrium boundary layer on the flat test wall. The cross section at the entrance of the test section is 0.91m in width and 0.25m in height, which are 11.67H and 3.21H respectively. The turbulence intensity observed was 0.1% and the potential core was uniform to within 0.5% in the spanwise and 1% in the vertical directions at the entrance of the test section for a nominal speed of U_{ref} = 27.5m/s.

The bump was mounted on the test wall in the center floor of the test section 3.03m from the entrance of the test section. Inserts for the wind tunnel sidewalls were constructed to minimize blockage-induced pressure gradients around the bumps. The Reynolds number Re_H based on the height H and U_{ref} at a temperature of 25±1°C is 1.3×10^5 for the large bump 3. When a given bump was not in place, a mean 2-D zero pressure gradient turbulent boundary layer 39mm thick was present with Re_θ equal to 7300.

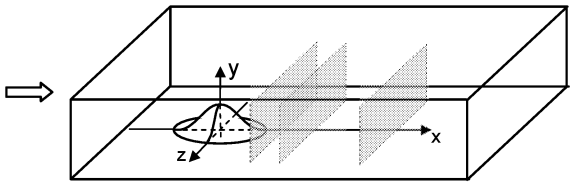

Figure 2. Schematic diagram of the tunnel test section and measurement planes at x/H=2.62, 3.63, 6.59

Velocity measurements were made using a computerized A.A. Lab System AN-1003 ten channel hot-wire anemometry system. Miniature Kovaznay type four-sensor hot-wire probes manufactured by Auspex Corporation (type AVOP-4-100) were used. The total measurement volume is approximately 0.5 mm^3. Anemometer bridges were optimized to give a matched frequency response greater than 15 kHz. A lookup table method described in detail by Wittmer et al. (1998) is used to calculate the three velocity components.

For time-averaged mean flow and turbulence measurements, at each measurement point 60 records of 1024 samples of hot-wire signal were recorded at a sampling frequency of 1600Hz. For spectral measurements, at each measurement point 60 records of 2^{18} samples were recorded at a rate of 25.6 kHz. The covered frequency range is from 0.1Hz to 12.8 kHz with a frequency resolution of 0.1 Hz.

RESULTS AND DISCUSSION

Mean Flow

To give context, the Byun and Simpson (2005) measurement results of the mean flow structure over large bump 3 are briefly reviewed. They found that there is a 3D saddle-focus separation structure on the lee side. The separation region is a thin layer with thickness of about 5mm (0.064H) starting at x/H=0.96 on the bump surface. The back flow stagnates there in the center plan and then moves outward in spanwise direction, rolling up and forming two counter-rotating foci at x/H=1.2 and z/H=±0.7. Their rotating direction is anti-clockwise at the positive z side and clockwise at the negative z side, appearing from both downstream and top.

Figures 3 present the mean flow downstream large bump 3 at three streamwise locations, x/H=2.62, 3.63, and 6.59 in terms of contours of U/U_{ref} , and the cross velocity vectors $(V,W)/U_{ref}$. These plots show the flow as it would appear from upstream. The 2D projection of the bump is also indicated in figures 3. These figures reveal that the flow rushes into from peripheral region to fill the room behind the bump and forms two flattened contour-rotating

vortices. The rotating direction of the vortices at each side is opposite to that of the corresponding vortices within the separation region on the lee side reported by Byun and Simpson (2005). An explanation to this is that the measurement locations are behind the possible reattachment location so the measured flow comes from the flow over the separation layer, and thus have opposite induced vorticity.

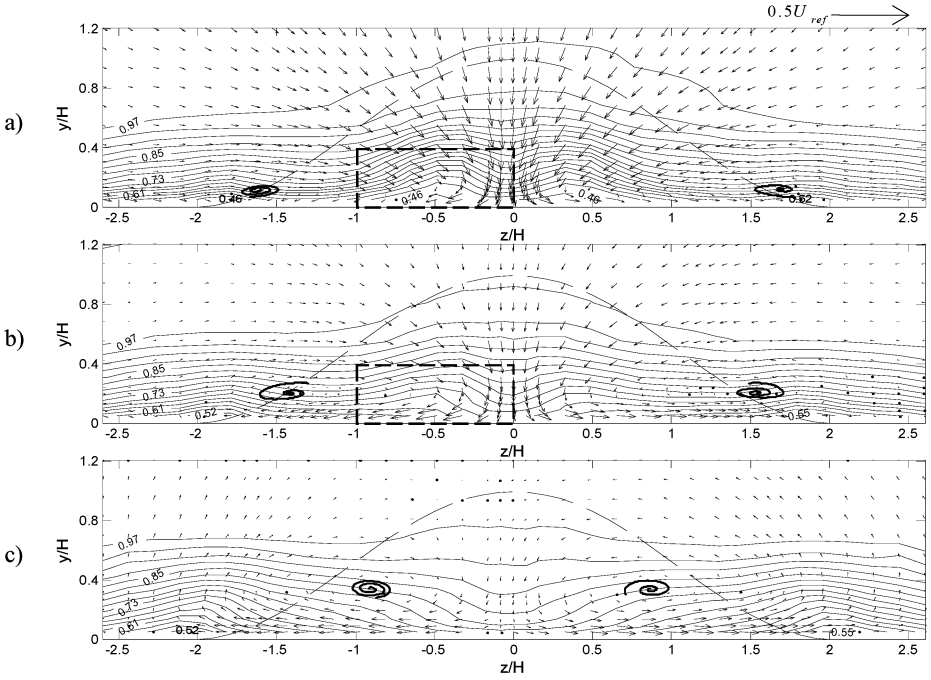

Figure 3. Mean flow field, a) *x/H*=2.62, b) *x/H*=3.63, c) *x/H*=6.59.
(Small pieces of streamline indicating centers of the secondary flow in measurement plans, dashed rectangles indicating regions where cross flow was rotated in figure 5)

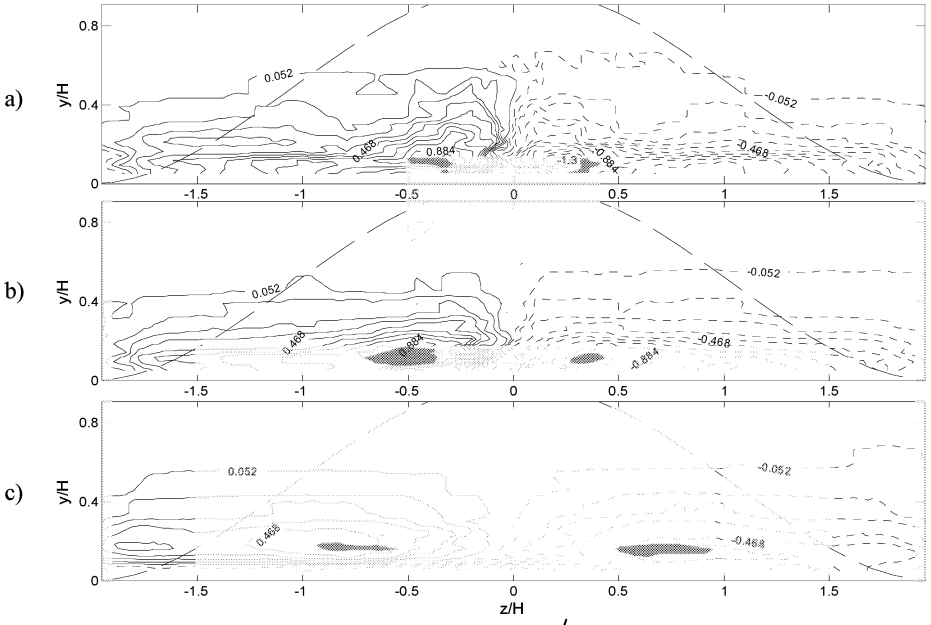

Figure 4. Contours of streamwise mean vorticity $\omega_x H / U_{ref}$, a) *x/H*=2.62, b) *x/H*=3.63, c) *x/H*=6.59
(grey regions indicating helicity density magnitude larger than 0.95 for a) and b), 0.9 for c), contours from -1.3 to 1.3 in step of 0.104, dotted line indicating negative value)

At x/H=2.62, the contours of U/U_{ref} show that near the wall the contours have a saddle-like shape symmetric to the centerline and with two major deficit regions of a maximum velocity deficit of $0.56U_{ref}$ located at about z/H=±0.5. Two other very small deficit regions with a maximum deficit of $0.54U_{ref}$ are also formed near the wall at z/H=±1.8, just outside the bump projection. The location of these two small deficit regions seems be coincident with the location of the two outside ends of the flattened vortices. At x/H=3.63, the two major deficit regions move outward horizontally with a much lower deficit due to the filling of the free-stream flow from the peripheral region. At x/H=6.59, the streamwise velocity near the centerline is even much higher than the undisturbed boundary layer. The fact that there is no self-similarity in the contour shapes at various streamwise locations suggests the flow is highly evolving and three-dimensional.

The cross velocity vectors display that, at x/H=2.62, there is a strong filling motion, with an averaged cross velocity of about $0.15\,U_{ref}$ associated with the motion, toward the center where the flow starts to stagnate and turn to both side symmetrically. At x/H=3.63, the filling motion starts to get weaker, and the averaged cross velocity associated with the motion is about $0.08\,U_{ref}$. But the horizontal outward motion near the wall gets stronger. Finally at x/H=6.59, the filling motion is very weak and the outward motion near the wall is stronger and dominates the flow.

In figure 4, the contours of mean streamwise vorticity component, $\omega_x H/U_{ref}$, reveal two flattened oval regions that are almost antisymmetric to the centerline, with positive vorticity on the left side and negative vorticity on the right side. The overall mean circulation of one of the vortices, computed on a rectangular path extending from (y/H, z/H) = (0.15, -2) to (0.8, 0), is respectively 0.28, 0.28, and $0.20\,U_{ref}H$ for x/H=2.62, 3.63, and 6.59.

It can be seen that the centers of the vortical structures of the secondary flow (indicated by small pieces of streamline in figures 3) are, however, located just along the bump projection and outward from the major streamwise velocity deficit regions and locations with streamwise vorticity peak. The major deficit regions appear to be almost coincident with the location of the two streamwise vorticity peaks, suggesting that two vortical structures are formed there. The normalized helicity density, defined as $\vec{\Omega}\cdot\vec{V}/\left|\vec{\Omega}\right|\left|\vec{V}\right|$ where $\vec{\Omega}$ and $\vec{V}$ are, respectively, the mean vorticity and velocity vectors, was thus used to track the center of the streamwise mean vortex. The normalized helicity density should reach 1 and -1 at the vortex centers. Unsurprisingly, the vortex center locations, indicated by the grey markers in figure 4 which are peak regions of helicity magnitude, are much consistent with those revealed by streamwise vorticity peak, as well as those locations of the major streamwise velocity deficit regions. These vortex centers are not revealed by the cross velocity vectors just because the vortex center paths are not perpendicular to the measurement planes.

To disclose the flow structure of these vortex centers, the cross velocity vectors there (within the rectangular region shown in figure 3a and 3b) were rotated by a pitch angle θ_z of -10° for x/H=2.62 and of -5° for x/H=3.63. The rotated cross velocity vectors shown in figure 5 clearly reveal there is a strong vortex there. The negative pitch angles mean that while the two vortex centers move outwards as flow goes to downstream, the center paths are pointing down and the downward tendency gradually reduces.

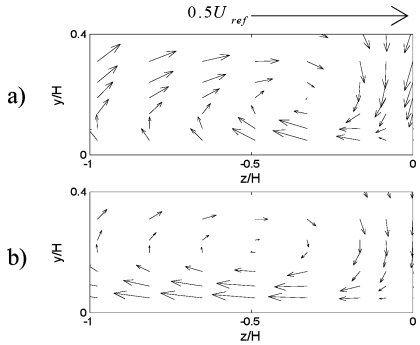

Figure 5. Cross flow vectors after a pitch-angle (θ_z) rotation, a) x/H=2.62, θ_z =-10°, b) x/H=3.63, θ_z =-5°

For the centers of the secondary flow shown in figure 3, the vortical structures there are very weak and the mean cross-flow velocities associated with its rotation are very small. As shown in next section, there is no footprint of high turbulence kinetic energy level existing at these center locations. These all suggest that they are produced actually by the filling motion of the flow, not by vortex shedding.

Turbulence Properties and Structure

The turbulence kinetic energy, $k = \overline{u_i'u_i'}/2U_{ref}^2$, and its transport velocity vectors, $\left(\overline{w'k'},\overline{v'k'}\right)/k'U_{ref}$, where $k' = u_i'u_i'/2U_{ref}^2$, at three locations for large bump 3 are plotted in figures 6. The t.k.e. contours are plotted in the same scale to reveal the decay. At x/H=2.62, the t.k.e. peak of 0.04 is located close to the centerline and $0.2H$ above the wall. As flow goes downstream, the t.k.e. peak forms a saddle-like structure. All of these contours have a symmetric double-peaked shape behind the bump. The location of t.k.e. peaks are quite consistent with that of the streamwise vorticity peaks.

To reveal the turbulence fluctuations, spectral data measured at five points along the centerline (y/H=0.07, 0.20, 0.36, 0.78, 1.20) at x/H=3.63 are presented in figures 7. Different ways were tried to scale the spectra data and $(U_d^2+V^2, U_{ref}/H)$ were finally found to be the best, where $U_d = U_{ref} - U$. All components of power spectra data collapse at high frequency except the freestream point y/H=1.2. This suggests that the high frequency turbulence

fluctuations at the centerline are dominated by the local defect velocity with the magnitude of $\sqrt{U_d^2 + V^2}$.

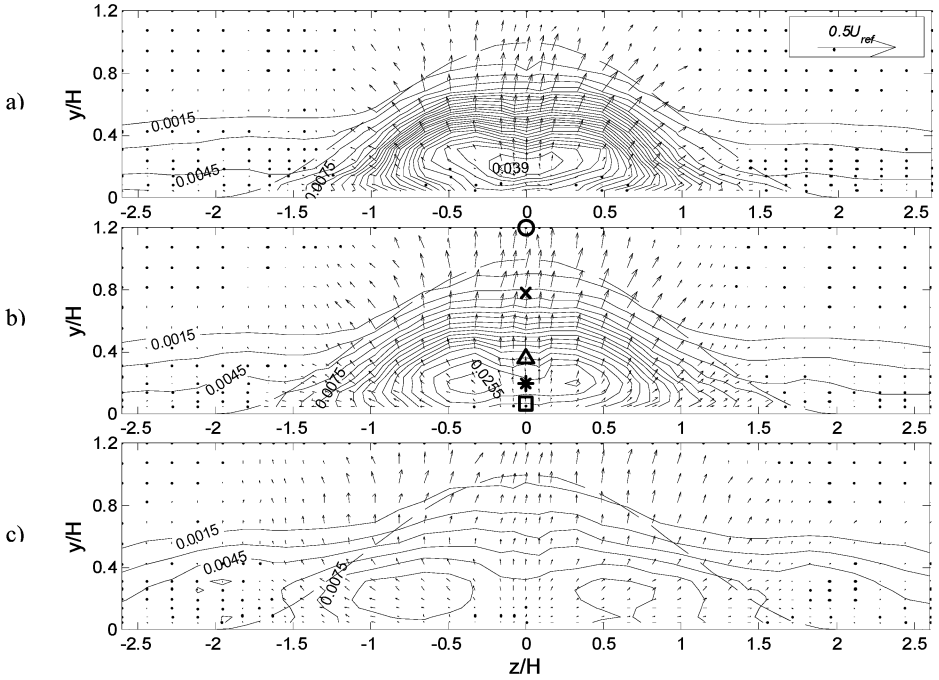

Figure 6. Contours and transport velocity vectors of turbulence kinetic energy
a) *x/H*=2.62, b) *x/H*=3.63, c) *x/H*=6.59. (contours from 0 to 0.04 in step of 0.0015, symbols at the centerline indicating the measurement locations of spectra shown in figures 7)

Another obvious feature is that there is a clear dividing line at normalized frequency of about 0.1, which is about 34Hz. This frequency is quite low and corresponds with a 10*H* moving distance at the freestream speed U_{ref} . Below this frequency, the spectra at the centerline clearly show that there are low frequency motions with large fluctuation magnitude. Above this frequency, almost all the spectra follow a power law to decay. For the G_{uu} component, the exponents were found to have a range from -1.7 for *y/H*=0.07 to -2.2 for *y/H*=1.2. Comparisons of the *u', v', w'* spectra over the inertial subrange show that they are unequal. This suggests that the flow is not isotropic.

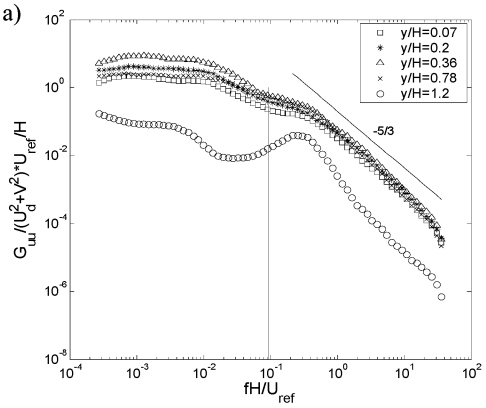

Figure 7. Spectra along the centerline at *x/H*=3.63, a) *u'* spectra

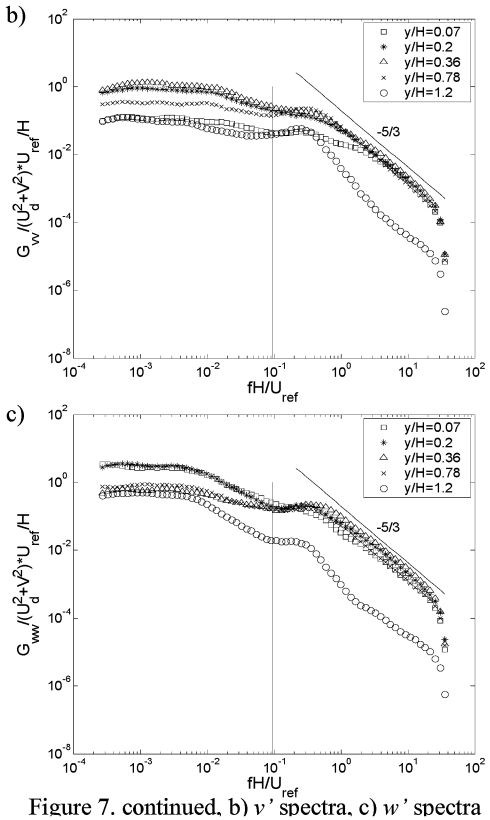

Figure 7. continued, b) *v'* spectra, c) *w'* spectra

The structures of the low frequency fluctuations are further revealed by spectral decomposition. The spectral data were integrated with respect to frequency up to 34Hz to obtain the contribution of low frequency fluctuation to the normal stresses. The shape and turbulence fluctuation level of these low frequency turbulence structures are shown in figure 8. The low frequency fluctuations occur mainly in streamwise direction behind the bump and spanwise direction near the wall.

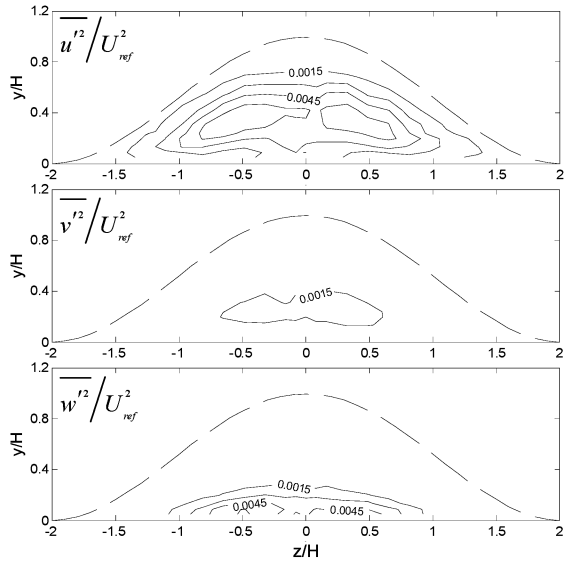

Figure 8. Contribution of low frequency fluctuation (f<34Hz) to normal stresses at x/H=3.63. (contours from 0 to 0.04 in step of 0.0015)

The integral length scales in streamwise direction were calculated by using $L_{u_i x} = UG_{u_i u_i}(0)/(4\overline{u_i'^2})$ to estimate the size of the structures. Figure 9 shows that the streamwise fluctuation of the structure has a maximum integral length of about $2.5H$ in the streamwise direction and the spanwise fluctuation near the wall has a maximum integral length of $1.5H$ in streamwise direction.

CONCLUSIONS

The three-dimensional axisymmetric bump generates highly evolving three-dimensional vortical flow pattern. There is strong downwash flow just behind the bump and outward flow near the wall away from the bump. The two vortex centers move outward and the center path has downward tendency just behind the bump. Large-scale and low frequency ($fH/U_{ref} < 0.1$) turbulence structures exist behind the bump in streamwise direction with an integral length of about $2H$ and in spanwise direction near the wall with an integral length of about H . This suggests that the downstream flow is dominated by the wake from the complicated separation.

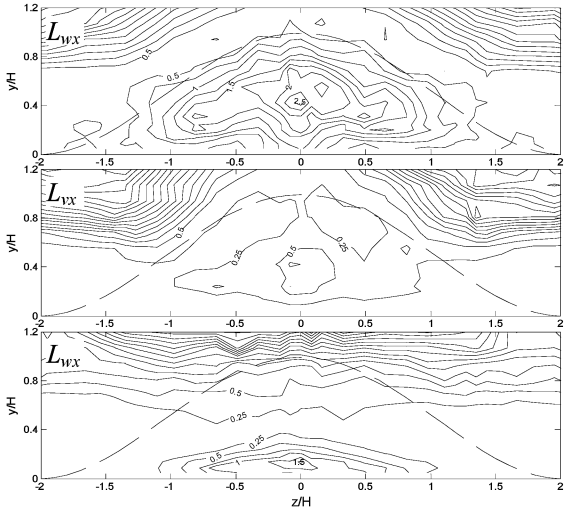

Figure 9. Integral length scales at x/H=3.63. (contours from 0 to $5H$ in step of $0.25H$)

ACKNOWLEDGEMENTS

The authors would like to thank the Office of Naval Research, in particular Dr. Ron Joslin, for support of this work through grant N00014-01-1-0421.

REFERENCES

Byun, G., Simpson, R. L., and Long, C. H., 2004, "Study of Vortical Separation from Three-Dimensional Symmetric Bumps," AIAA Journal, Vol. 42, No. 4, pp. 754-765.

Byun, G., and Simpson, R. L., 2005, "Structure of Three-Dimensional Separated Flow on an Axisymmetric Bump," AIAA Paper 2005-0113, 43rd Aerospace Science Meeting an Exhibit, Jan. 10-13, Reno, NV.

Devenport, W. J., and Simpson, R. L., 1990, "Time-Dependent and Time-Averaged Turbulence Structure Near the Nose of a Wing-Body Junction", Journal of Fluid Mechanics, Vol. 210, pp. 23-55.

Patel, N., Stone, C., and Menon, S., 2003, "Large-Eddy Simulation of Turbulent Flow Over an Axisymmetric Hill," AIAA Paper 2003-0967.

Simpson, R. L., Long, C. H., and Byun, G., 2001, "Study of Vortical Separation From an Axisymmetric Hill," 2nd Turbulent Shear Flow Phenomena Symposium, Stockholm, Sweden, June 27 - 29, Vol. III, pp.65-70; also Int. J. Heat & Fluid Flow, Vol. 23, pp. 582 – 591, 2002.

Wang, C., Jang, Y. J., and Leschziner, M. A., 2004, "Modelling two- and three-dimensional separation from curved surfaces with anisotropy-resolving turbuelcne closures," International Journal of Heat and Fluid Flow, 25, pp. 499-512.

Willits, S. M., and Boger, D. A., 1999, "Measured and Predicted Flows Behind a Proturberance Mounted on a Flat Plate," Applied Research Laboratory, Penn State University

Wittmer, K. S., Devenport, W. J., and Zsoldos, J. S., 1998, "A Four-Sensor Hot-wire Probe System for Three-component Velocity Measurement," Experiments in Fluids, Vol. 24, pp. 416.